Targeting G protein-coupled receptors with magnetic carbon nanotubes

Pineux, Florent; Federico, Stephanie; Klotz, Karl-Norbert; Kachler, Sonja; Michiels, Carine; Sturlese, Mattia; Prato, Maurizio; Spalluto, Giampiero; Moro, Stefano; Bonifazi, Davide

Published in:
ChemMedChem

DOI:
10.1002/cmdc.202000466

Publication date:
2020

Document Version
Peer reviewed version

FULL PAPER

Targeting G protein-coupled receptors with magnetic carbon nanotubes: The A_3 adenosine receptor case

Florent Pineux,[a] Stephanie Federico,*[b] Karl-Norbert Klotz,[c] Sonja Kachler,[c] Carine Michiels,[d] Mattia Sturlese,[e] Maurizio Prato,[b,f] Giampiero Spalluto,[b] Stefano Moro,[e] and Davide Bonifazi *[g]

[a] Dr. F. Pineux
Department of Chemistry and Namur Research College (NARC)
University of Namur
Rue de Bruxelles 61, 5000 Namur, Belgium
[b] Dr. S. Federico, Prof. G. Spalluto
Dipartimento di Scienze Chimiche e Farmaceutiche
Università degli Studi di Trieste
Via L.Giorgeri 1, 34127 Trieste, Italy
E-mail: sfederico@units.it
[c] Prof. K.-N.Klotz
Institut für Pharmakologie und Toxikologie
Universität Würzburg
Versbacher Straße 9, 97078 Würzburg, Germany
[d] Dr. C. Michiels
Namur Research Institute for Life Science (NARILIS), Unité de Recherche en Biologie Cellulaire (URBC)
University of Namur
B - 5000 Namur, Belgium
[e] Dr. M. Sturlese, Prof. S. Moro
Dipartimento di Scienze del Farmaco, Molecular Modeling Section (MMS)
Università degli Studi di Padova
Via F. Marzolo 5, 35131 Padova, Italy
[f] Prof. M. Prato
Carbon Nanobiotechnology Laboratory
CIC BiomaGUNE
Paseo de Miramón 182, 2009 Donostia-San Sebastián, Spain
[g] Prof. D. Bonifazi
Institut für Organische Chemie
Universität Wien
Währinger Str. 38, 1090 Wien
E-mail: davide.bonifazi@univie.ac.at

Supporting information for this article is given via a link at the end of the document.

Abstract: A_3 adenosine receptor (AR) is a G protein-coupled receptor (GPCR) overexpressed in the membrane of specific cancer cells. Thus, the development of nanosystems targeting this receptor could be a strategy to both treat and diagnose cancer. Fe-filled carbon nanotubes (CNTs) are an optimal platform for theranostic purposes, and the use of a magnetic field can be exploited for cancer magnetic cell sorting and thermal therapy. In this work, we have conjugated an A_3AR ligand on the surface of Fe-filled CNTs with the aim to target cells overexpressing A_3ARs. In particular, two conjugates bearing PEG linkers of different length were designed. A docking analysis on the A_3AR showed that both CNT and linker do not interfere with ligand binding to the receptor, that was confirmed by *in vitro* preliminary radioligand competition assays on A_3AR. Encouraged by this result, magnetic cell sorting was applied to a mixture of cells overexpressing or not the A_3AR where our compound displayed indiscriminate binding to all cells. Despite this, it is the first time that a GPCR ligand was anchored to a magnetic nanosystem, thus it opens the door to new applications for cancer treatment.

Introduction

Adenosine is a purine nucleoside that mediates numerous essential physiological functions by interacting with adenosine receptors (ARs), which belong to the family of G-protein-coupled receptors (GPCR).[1] Adenosine is involved in neuronal, cardiac and immune processes, as well as in inflammation and cancer.[2–5] Four different ARs subtypes have been discovered to date and classified as A_1, A_{2A}, A_{2B} and A_3.[6] High extracellular adenosine concentration (in the micromolar range), which is able to stimulate all the AR subtypes, is commonly found in the tumor microenvironment due to hypoxia or cell damages.[7,8] Cells generally co-express multiple AR subtypes on their membrane and their specific response to adenosine is dictated by a particular AR expression pattern.[9] The precise role of A_3AR in tumor development is not yet fully clarified. Whereas on one hand A_3AR stimulation has been found to inhibit prostate carcinoma cells proliferation and induce cell death in myeloid and lymphoid cell lines,[10,11] it has been shown on the other hand that such stimulation could enhance glioblastoma cell invasion and favour colon tumour cell proliferation.[12,13] Also, A_3AR has been found to be up-regulated (up to 2.3 fold compared to normal tissues) in a wide range of tumours such as colon, prostate or skin carcinoma.[10,14,15] Moreover, it has been shown that A_3AR

expression levels directly correlate to cancer severity.[16,17] Therefore, the A_3AR could be considered as a marker for this kind of tumours and it is possible to take advantage of this to develop therapeutic and/or diagnostic systems able to specifically target this receptor.

The demonstration of the existence of ARs dimers and oligomers makes ARs an attractive target for multivalent nanoparticles.[18–20] In fact, the presence of multiple ligands on the same platform could bridge the different binding sites present in GCPR multimeric architectures. The resulting stabilization of the system could ameliorate or lead to different pharmacodynamics and pharmacokinetic properties in comparison to the monomeric ligands.[21] In this respect, Jacobson and co-workers developed a series of polyamidoamine (PAMAM) dendrimers displaying multiple AR ligands.[21–26] In particular, when an A_3 ligand was conjugated to a G4 PAMAM dendrimeric core, a dramatic enhancement of both selectivity and affinity was achieved when compared to the ligand alone.[25] Gold nanoparticles were also used as platforms to modulate adenosine receptors by conjugation with both agonists and antagonists.[27] Moreover, the use of multivalent nanostructures allows the integration of other relevant components for therapeutic, diagnostic and monitoring purposes.[24,28,29]

In this context, carbon nanostructures, and in particular carbon nanotubes (CNTs) have been proposed as complementary multifunctional nanostructures in nanomedicine for imaging, tissue engineering, drug delivery and anticancer platforms.[30–39] Particularly appealing are Fe-filled carbon nanotubes (Fe@CNTs), as they display multimodal functionality for filtration/separation of biological species, magnetic drug-targeting and/or delivery, magnetic resonance imaging, and localized magnetic fluid hyperthermia-based treatments.[40–42] Recently, our group used Fe@CNTs conjugated with the antibody Cetuximab targeting a plasma membrane receptor (EGFR) overexpressed in cancer cells.[43] *In vitro* experiments showed that the magnetic hybrids efficiently sort cancer cells from populations of healthy cell lines and selectively suppress them through magnetic fluid hyperthermia (MFH) upon application of an alternating magnetic field.[44] Building on these results, in this work we report on the use of Fe@CNTs conjugates for targeting A_3AR. Fe@CNTs were conjugated to a A_3AR antagonist (**1**) with a pyrazolo[4,3-*e*]-1,2,4-triazolo[1,5-*c*]-pyrimidine (PTP) core (Fig. 1), which contemporary bears a conjugable carboxylic group and a good affinity and selectivity towards A_3AR at the same time.[45] Competition binding assays were performed to evaluate the affinity of Fe@CNTs-PEG-PTP for A_3ARs. Finally, derivatives were used for preliminary *in vitro* evaluation of their magnetic sorting effectiveness of cells overexpressing A_3AR.

Figure 1. Structure of the potent A_3 AR antagonist **1** and of the conjugate with Fe@CNTs (**2**,**3**).

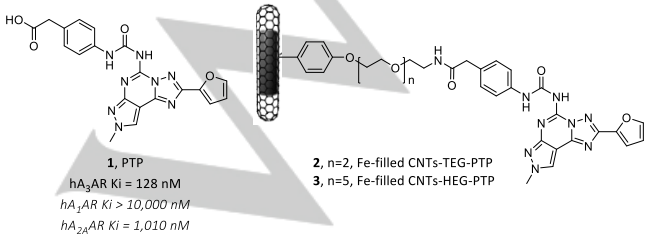

Results and Discussion

Bioconjugation approach and design

The replacement of a large water-solubilizing protein (antibody) by a smaller hydrophobic ligand (A_3AR antagonist) suggests to use water solubilizing linkers such as polyethylene glycol (PEG) chains between the Fe@CNT surface and antagonist **1**, this in order to enhance conjugate water solubility. Besides the positive effect of keeping good dispersion properties, PEG chains act as spacers to avoid the disruption of the ligand affinity towards A_3AR by a potential steric clash. Two PEG chains were used (tri- or hexaethyleneglycol, TEG or HEG) to study the steric impact on the conjugate properties (**2**,**3**). The synthetic route towards Fe@CNTs-PEG-PTP derivatives **2** and **3** can be divided into two parts: first, the synthesis of aniline linkers **4** and **5** (Scheme 1), and second the covalent grafting onto the Fe@CNTs. This allows the subsequent conjugation of CNTs with PTP carboxylic acid ligand **1** (Scheme 2). In order to assess the perturbation on the A_3AR affinity caused by the presence of the PEG, we also synthetized (Scheme S1) references TEG-PTP (**6**) and HEG-PTP (**7**).

Computational validation of the CNT-based architecture

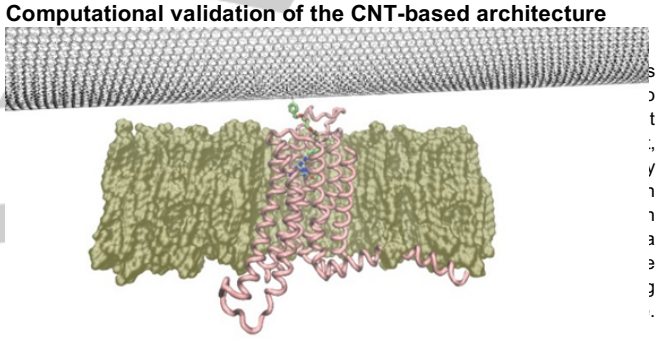

Figure 2. *In silico* model of CNT-HEG-PTP bound to hA_3AR. HEG-PTP are colored with green carbon atoms while the A_3AR receptor is displayed as a pink ribbon. Only a section of the POPC bilayer (gold surface) is showed to facilitate the receptor visualization.

Finally, to mimic the presence of the cell membrane, the complex was embedded in a phosphatidylcholine bilayer. The whole system (Fig. 2) shows that the CNT framework does not affect the PTP binding. One should also note that the PEG linker does not guarantee wide freedom in the PTP mobility, that could be eventually restored by further extending the PEG linker.

Synthesis of aniline linkers

The synthesis of anilines **4** and **5** started with the mono-tosylation of commercially available triethylene (TEG) and hexaethylene (HEG) glycols. In the first case, affordable TEG was used in large excess (8 eq.) affording mono-tosylated TEG **8** in near-quantitative yield. On the other hand, the expensive HEG substrate was reacted in stoichiometric amounts with tosyl chloride, using Et_3N as a base, to give desired mono-tosylated HEG **9** in modest yield (34%) due to the unavoidable formation of the bis-tosylated derivative. Molecules **8** and **9** were reacted with NaN_3 in DMF, to generate azides **10** and **11** in excellent yields (80% and quantitative, respectively). Subsequent tosylation of the remaining hydroxyl functionality, gave compounds **12** and **13** that, followed by Williamson etherification with *p*-nitrophenol, were transformed into nitro derivatives **14** and **15** in very good yields (85% and 92%, respectively) over the two steps. Simultaneous

reduction of both azido and nitro groups with H_2 and Adam's catalyst (PtO_2) gave the amine derivatives **16** and **17** in very good yields (94% and 92%, respectively). Building on the different reactivity of the terminal alkyl amines compared to arylamines, chemoselective protection of compounds **16** and **17** with BOC-anhydride afforded **4** and **5** in good yields (66 and 69%, respectively). Small amounts (7%) of bis-protected HEG by-product **18** were also isolated, whereas bis-protected TEG derivative was detected in a small amount in the reaction mixture and not isolated.

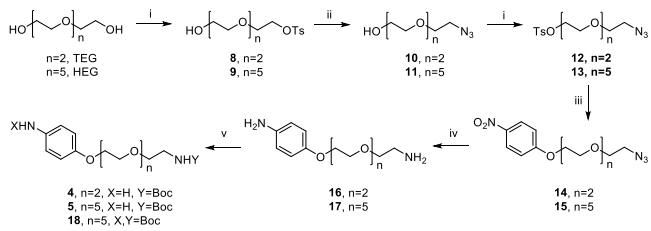

Scheme 1. Synthesis of aniline linkers **4** and **5**. Reagents and conditions: i) TsCl, KOH, dichloromethane, 0 °C to r.t., 8 h; ii) NaN_3, DMF, 60 °C, overnight; iii) *p*-nitrophenol, K_2CO_3, DMF, 60 °C, overnight; iv) PtO_2 (1 mol %), H_2 (1 atm), methanol, r.t., overnight; v) Boc_2O, THF, r.t., 16 h.

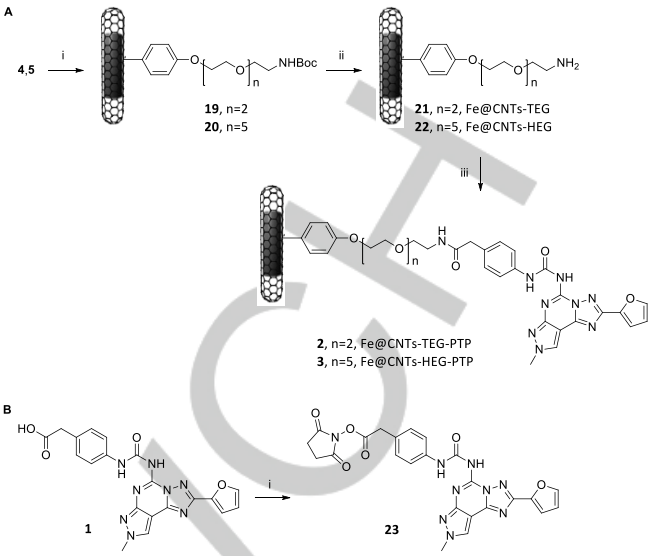

Scheme 2. Synthesis of Fe@CNTs-PEG-PTP systems (**2**,**3**). A. Reagents and conditions: i) Fe filled CNTs, isoamyl nitrite, NMP, 90 °C, 20 h; ii) HCl, methanol, r.t., 16 h; iii) **23**, DMF, TEA, r.t., 14 h. B. Reagents and conditions: i) NHS, EDC.HCl, DMAP, DMF, r.t., 48 h.

In a second stage, anilines **4** and **5** were grafted onto raw Fe@CNTs under the conditions described by Tour and coworkers,[[48]] i.e. *in-situ* reaction with isoamyl nitrite and CNTs, giving respectively Fe@CNTs-TEG-NHBoc (**19**) and Fe@CNTs-HEG-NHBoc (**20**) (Scheme 2).

A test reaction was performed on linker **5** to check the BOC-deprotection conditions. It was found that using a 1.5 M solution of HCl in MeOH and water was sufficient to achieve a complete BOC deprotection in one night at rt. Fe@CNTs-PEG-NHBoc derivatives **19** and **20** were deprotected into corresponding Fe@CNTs-PEG-NH_2 derivatives **21** and **22**. All four CNT derivatives (**19**-**22**) were characterized by XPS, revealing new peaks at 400.0 eV attributed to the N 1s binding energy of the amino-terminated PEG chains (Figs. 3C-3D). Grafting of PEG linkers provoked a doubling of detected O 1s atomic percentages (from about 3 to 6 %, Table 1) in Fe@CNTs-PEG-NHBoc (**19**,**20**) and Fe@CNTs-PEG-NH_2 (**21**,**22**) compared to pristine Fe@CNTs.

Linkers grafting onto Fe@CNTs

In a second stage, anilines **4** and **5** were grafted onto raw Fe@CNTs under the conditions described by Tour and coworkers,[[48]] i.e. *in-situ* reaction with isoamyl nitrite and CNTs, giving respectively Fe@CNTs-TEG-NHBoc (**19**) and Fe@CNTs-HEG-NHBoc (**20**) (Scheme 2).

A test reaction was performed on linker **5** to check the BOC-deprotection conditions. It was found that using a 1.5 M solution of HCl in MeOH and water was sufficient to achieve a complete BOC deprotection in one night at rt. Fe@CNTs-PEG-NHBoc derivatives **19** and **20** were deprotected into corresponding Fe@CNTs-PEG-NH_2 derivatives **21** and **22**. All four CNTs derivatives (**19**-**22**) were characterized by XPS, revealing new peaks at 400.0 eV attributed to the N 1s binding energy of the amino-terminated PEG chains (Figs. 3C-3D). Grafting of PEG linkers provoked a doubling of detected O 1s atomic percentages (from about 3 to 6 %, Table 1) in Fe@CNTs-PEG-NHBoc (**19**,**20**) and Fe@CNTs-PEG-NH_2 (**21**,**22**) compared to pristine Fe@CNTs.

TGA (thermogravimetric analysis) measurements performed under air also evidenced a successful functionalization of the carbon framework, displaying an enhanced weight loss of about 4-5 wt% at 400 °C compared to pristine Fe@CNTs (Fig. 4), after a pyrolysis event occurring between 200 and 350 °C for Fe@CNTs-PEG-NHBoc (**19**,**20**) and Fe@CNTs-PEG-NH_2 (**21**,**22**). This pyrolysis event can be related to the thermal decomposition of the PEG chain as it is retrieved in the TGA analysis of reference Boc-HEG-aniline **5** (Fig. 4B). Precise quantification of the functionalization degree based on a triplicate of TGA runs per compound was attempted (Table 1) and gave values of 356 ± 75 and 186 ± 49 μmol·g^{-1} for Fe@CNTs-TEG-NH_2 (**21**) and Fe@CNTs-HEG-NH_2 (**22**), respectively. As the values obtained by TGA showed a high variability (RSD > 21%), we performed complementary elemental analyses (Table 1) to obtain a free amino group content of 109 ± 7 and 88 ± 0 μmol·g^{-1} for CNTs-TEG-NH_2 (**21**) and Fe@CNTs-HEG-NH_2 (**22**), respectively.

Conjugation of A_3AR antagonist to Fe@CNTs-PEG-NH_2

PTP was firstly reacted with N-hydroxysuccinimide (NHS) in the presence of catalytic amount of DMAP,[[45]] to afford NHS activated ester **23** in 44% yield (Table S1, entry 2; Scheme 2B). It is important to note that NHS ester **23** is rather unstable either as a solid or dissolved in DMSO and was consequently synthesized and isolated only in the required amounts and directly conjugated to Fe@CNTs-PEG-NH_2 derivatives (**21**,**22**).

Amide reaction coupling between **23** and the Fe@CNTs-PEG-NH_2 derivatives (**21**,**22**) in DMF in the presence of Et_3N yielded final bioconjugates Fe@CNTs-TEG-PTP (**2**) and Fe@CNTs-HEG-PTP (**3**) (Scheme 2A).

The conjugation of PTP **1** to Fe@CNTs-PEG-NH_2 (**21**,**22**) was confirmed and quantified by a combination of XPS (X-ray photoelectron spectroscopy), TGA and EA (elemental analysis) techniques. In particular, XPS survey spectra displayed a substantial 2-fold increase in the N 1s atomic percentages when passing from Fe@CNTs-PEG-NH_2 (**21**,**22**) to Fe@CNTs-PEG-PTP (**2**,**3**) (Table 1). The XPS spectra of Fe@CNTs-PEG-PTP

conjugates **2** and **3** display a peak centered at 399.5 eV with a shoulder at 401.0 eV in the N 1s region. This shape is a signature of the presence of PTP ligand **1** (Fig. 3).

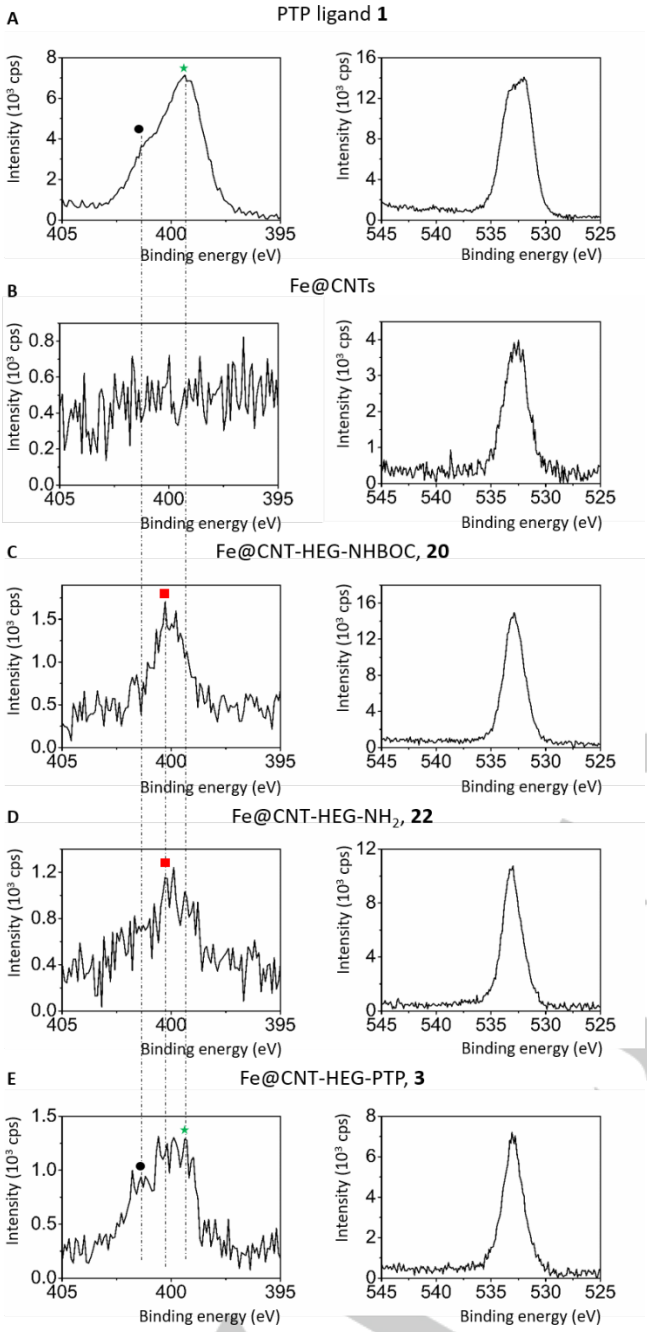

Figure 3. N 1s (left) and O 1s (right) XPS spectra of PTP ligand **1** (A), Fe@CNTs (B), Fe@CNTs-HEG-NHBOC **20** (C), Fe@CNTs-HEG-NH_2 **22** (D) and Fe@CNTs-HEG-PTP **3** (E). Peak maximum of PTP **1** is denoted with a green star (399.5 eV) and the "shoulder' with a black dot (401.0 eV). Peak maxima of Fe@CNTs-HEG-NHBOC **20** and Fe filled-CNTs-HEG-NH_2 **22** are denoted with a red square (400 eV).

TGA of Fe@CNTs-PEG-PTP (**2**,**3**) performed under air showed the presence of two additional pyrolysis events compared to Fe@CNTs-PEG-NH_2 (**21**,**22**) (Fig. 4) at 280 °C and 350 °C which are also retrieved in the TGA profile of ligand **1**. Attempts to estimate the PTP content in Fe@CNTs-PEG-PTP derivatives (**2**,**3**) over three TGA runs were affected by high variability (RSD > 63%). To reach a better precision, the elemental composition of Fe@CNTs-PEG-NH_2 (**21**,**22**) and Fe@CNTs-PEG-PTP (**2**,**3**) was determined by EA on duplicates, obtaining values associated with low RSD (> 3%). The increase in N-content related to the conjugation of **1** was employed to estimate the loading of PTP (Table 1). Interestingly, we have observed by this technique that Fe@CNTs-HEG-PTP (**3**) display about two times more PTP ligand (34.0 ± 0.7 $\mu mol \cdot g^{-1}$) than do Fe@CNTs-TEG-PTP (**2**, 16.1± 0.5 $\mu mol \cdot g^{-1}$). The estimate unreacted fractions of amino groups in Fe@CNTs-TEG-PTP (**2**) and Fe@CNTs-HEG-PTP (**3**) were 85% and 61%, respectively.

Table 1. XPS, TGA and EA characterization data for Fe@CNTs, Fe filled-CNTs-PEG-NH_2 **21**,**22** and Fe filled-CNTs-HEG-PTP **2**,**3**. XPS atomic percentages were calculated on spectra recorded from three different spots of the same sample and expressed as mean ± S.D. N wt% were measured by EA and are the average of duplicates. n.d.: not detected. n.a.: not applicable.

Cmpd	XPS C 1s[a] (%)	XPS N 1s[a] (%)	XPS O 1s[a] (%)	TGA Free amines ($\mu mol \cdot g^{-1}$)	TGA PTP ($\mu mol \cdot g^{-1}$)	EA Free amines ($\mu mol \cdot g^{-1}$)	EA PTP ($\mu mol \cdot g^{-1}$)
CNTs	97.11 ± 0.52	n.d.	2.89 ± 0.52	n.a.	n.a.	0.0 ± 0.0	n.a.
21	92.42 ± 0.42	1.28 ± 0.17	6.29 ± 0.28	356 ± 75	n.a.	109.0 ± 7.0	n.a.
22	92.32 ± 1.41	1.53 ± 0.11	6.15 ± 1.39	186 ± 49	n.a.	88.3 ± 0.0	n.a.
2	89.39 ± 0.77	2.78 ± 0.22	7.82 ± 0.69	336 ± 78	20 ± 22	92.9 ± 7.0[b]	16.1 ± 0.5
3	88.71 ± 0.33	3.11 ± 0.37	8.18 ± 0.10	32 ± 109	154 ± 97	54.3 ± 0.7 [b]	34.0 ± 0.7

[a] Electron configuration of the detected electron within the atom.

[b] Difference between initial free amines and PTP contents.

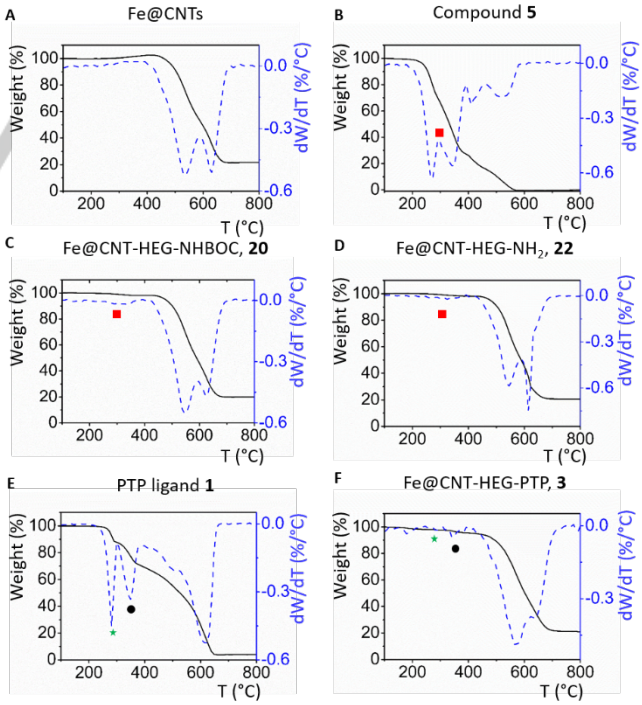

Figure 4. TGA profiles under air displayed as temperature-modulated weight% (——) and differential weight% (----) of (A) Fe@CNTs, (B) compound **5**, (C) Fe@CNTs-HEG-NHBOC **20**, (D) Fe@CNTs-HEG-NH_2 **22**, (E) PTP ligand **1**, and (F) Fe@CNTs-HEG-PTP **3**. The pyrolysis event associated with the decomposition of the PEG chain is indicated with a red square and those

associated with decomposition of ligand **1** with a green star (280 °C) and a black circle (350 °C).

Competition binding experiments of Fe@CNTs-PEG-PTP on the A_3AR

In order to evaluate the ability of the Fe@CNTs-PEG-PTP conjugates to target A_3ARs, preliminary binding experiments to determine their affinity to the receptor were carried out (Fig. 5).

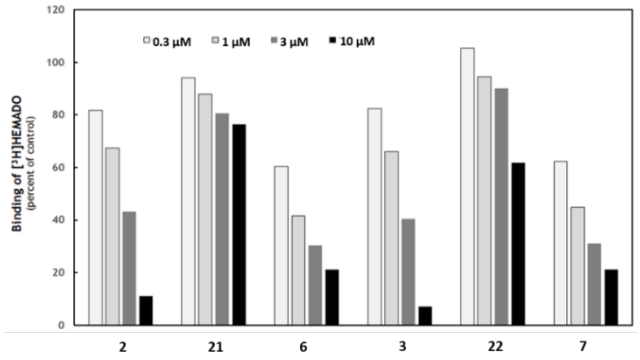

Figure 5. Preliminary displacement binding experiments of Fe-filled-CNTs-TEG-PTP (**2**), Fe-filled-CNTs-TEG-NH_2 (**21**), TEG-PTP (**6**), Fe-filled-CNTs-HEG-PTP (**3**), Fe-filled-CNTs-HEG-NH_2 (**22**) and HEG-PTP (**7**), at different concentrations: 0.3, 1, 3 and 10 µM (for CNTs the concentrations are based on calculated PTP content or on the same weight amount as for the derivatized material for control Fe filled-CNTs-PEG-NH_2). N = 1 for all conditions.

Succinctly, these tests measure competition of Fe@CNTs-PEG-PTP conjugates (**2**,**3**) for binding of a radioactively labeled A_3AR selective agonist, [^{3}H]HEMADO at human A_3ARs. Reference measurements were performed with Fe@CNTs-PEG-NH_2 derivatives **21** and **22**, and with TEG-PTP and HEG-PTP comparators **6** and **7** (Scheme S1).[[49,50]] The different concentrations studied were 0.3, 1, 3 and 10 µM. For the CNT bioconjugates, the concentrations were estimated on calculated PTP content and the reference Fe@CNTs-PEG-NH_2 (**21**,**22**) were tested using the same weight. Fig. 5 depicts the results of the [^{3}H]HEMADO displacement experiments. Clearly, both Fe@CNTs-TEG-PTP (**2**) and Fe@CNTs-HEG-PTP (**3**) compete efficiently with the radioligand.

Looking at 10 µM, one can see that Fe@CNTs-PEG-PTP **2** and **3** displaced more [^{3}H]HEMADO (about 90%) than non-targeting Fe@CNTs-PEG-NH_2 (**21**,**22**), although some non-specific binding interactions were observed with **19** and **20** as well. Interestingly, our Fe@CNTs-PEG-PTP (**2**,**3**) were more potent than comparators TEG-PTP **6** and HEG-PTP **7** at 10 µM. Finally, the *Ki* values of PEGylated derivatives TEG-PTP **6** and HEG-PTP **7** were 322 and 531 nM (preliminary data, n=1), respectively. These values are not so far from *Ki* value of the parent compound **1** (128 nM),[45] meaning that PEG chains have a negligible effect on the binding affinity of PTP towards human A_3AR.

Magnetic cell sorting effectiveness of Fe@CNTs-PEG-PTP

In-vitro biological assessment of the ability of Fe@CNTs-HEG-PTP (**3**) to fish out targeted cells was carried out. Specifically, Fe@CNTs-HEG-PTP (**3**) were mixed with either stable transfected A_3AR-overexpressing CHO cells or wild-type CHO cells (Figs. 6 and7) and the resulting suspension submitted to a static magnetic field. Surprisingly, we observed that both cell lines were extensively removed from the medium with a strong preference for the non-targeted CHO WT. To gain more insights into the binding mode of Fe@CNTs-HEG-PTP (**3**), we also tested their ability to fish human epidermoid carcinoma cells (A431) and human endothelial EA.hy926 cells (EA) (Figs. 6 and 7) as negative controls. A431 cells were chosen because they were reported to not overexpress A_3AR[4] and EA cells because they are no cancer cells. Interestingly, we observed that A431 cells were removed faster and to a higher extent than EA cells. In parallel, the selective magnetic removal of A_3AR+ vs. A_3AR- cells in a mixture was assayed by confocal fluorescence microscopy. Specifically, CHO cells were fluorescently stained with different colours (green for CHO WT and red for CHO A_3AR), mixed with Fe@CNTs-HEG-PTP **3** and placed against a magnet for 8 minutes (Fig. 8).

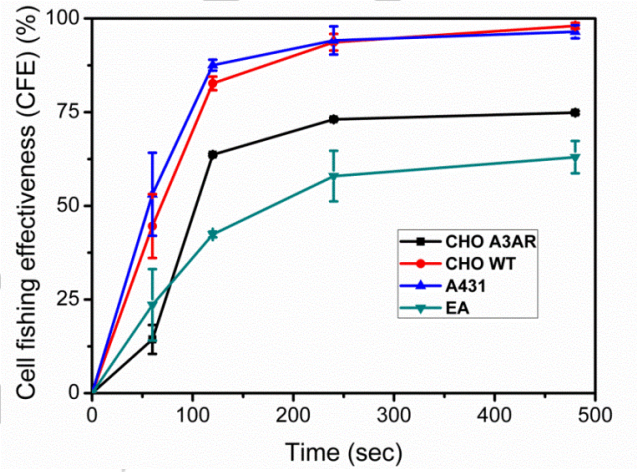

Figure 6. Magnetic cell sorting effectiveness (CFE) of CHO A_3AR (n=2), CHO WT (n=3), A431 (n=3) and EA (n=3) cells by Fe filled-CNTs-HEG-PTP (**3**). Results are expressed as mean ± S.D. The magnetic cell sorting effectiveness is defined as the percentage of cells fished out of a solution upon application of a given static magnetic field gradient at a given time.

We observed that both cell lines were removed, with only a few cells remaining in the supernatant after the magnetic manipulation. As a further control, the same experiment was repeated with non-targeting Fe@CNTs-HEG-NH_2 derivative **22** (Fig. 8). Under these conditions, we noted the nearly complete absence of both A_3AR and WT CHO cells in the supernatant after 8 minutes of magnetic filtration, suggesting that an enhanced cell binding and removal could be achieved compared to Fe@CNTs-HEG-PTP **3**. Together, these results suggest that Fe@CNTs-HEG-PTP **3** possess a high degree of non-specific binding. Interestingly, the preferential binding of Fe@CNTs-HEG-PTP **3** to A431 cells compared to EA cells along with the presence of remaining cationic free amino groups, suggests an important role played by electrostatic interactions. The enhanced non-specific magnetic fishing with Fe@CNTs-HEG-NH_2 **22** is in line with this hypothesis as it could be ascribed to their higher content in cationic amino groups compared to Fe@CNTs-HEG-PTP (**3**). Also, previous works reported a high level of adsorption of positively-charged nanoparticles on negatively-charged mammal cell surfaces or negatively-charged model membranes.[[51,52],[53]] In particular, Soukos *et al.* observed a preferential adsorption of cationic

polylysine polymers onto A431 cells compared to EA cells, in agreement with our observations.[52] This binding selectivity has been attributed to the overexpression of anionic polysialic acid residues in cancer cell membranes compared to other type cell models.[51] In addition, even if compounds **3** and **22** were incubated with cells for a very short time, an indiscriminate uptake of CNTs by cells could not be excluded. Thus, this could be another reason explaining the lack for selectivity of synthesized structures.

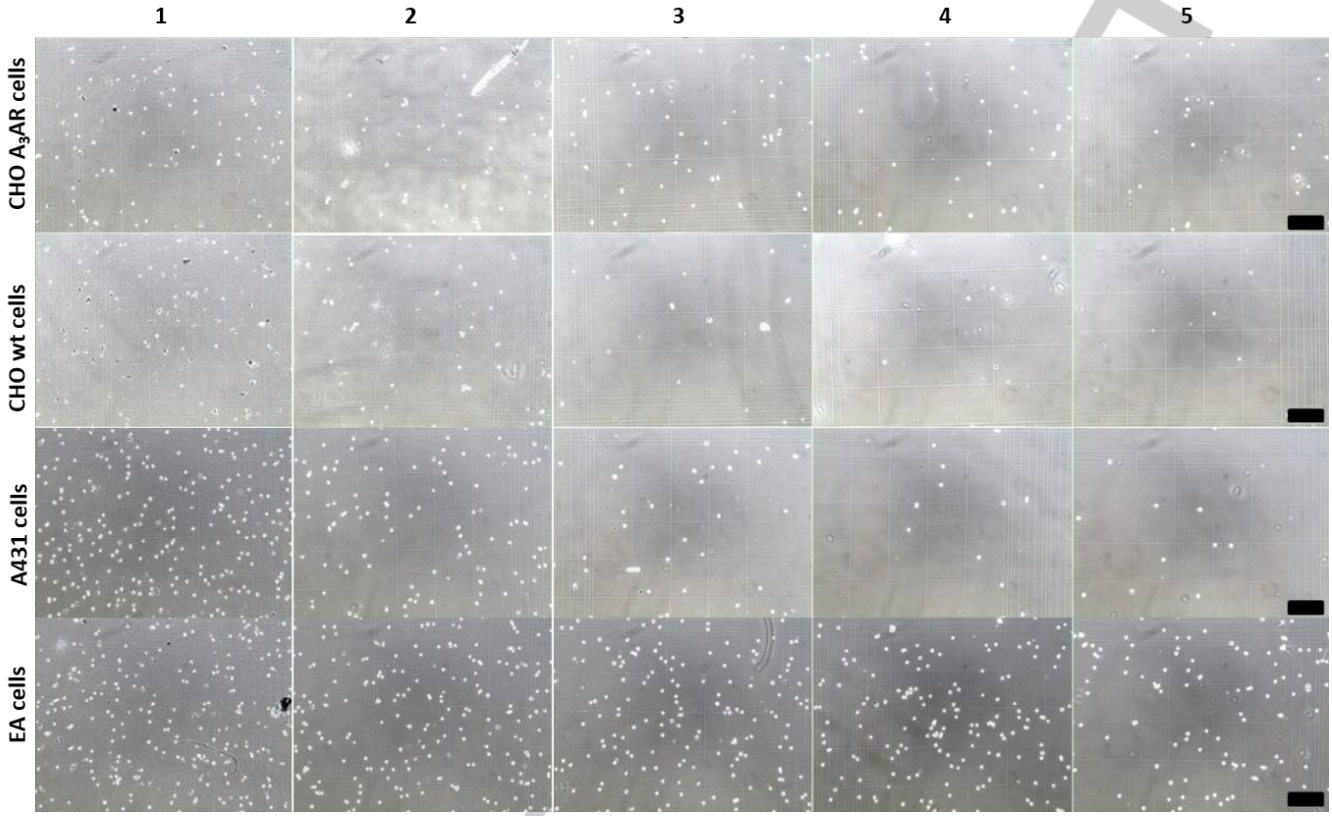

Figure 7. Optical microscopy images showing the cell density in the supernatant after 0 (1), 60 (2), 120 (3), 240 (4) and 480 (5) seconds of magnetic sorting of CHO A_3AR, CHO WT, A431 and EA cells by Fe@CNTs-HEG-PTP **3**. Scale bar = 250 μm (all the images are at the same scale).

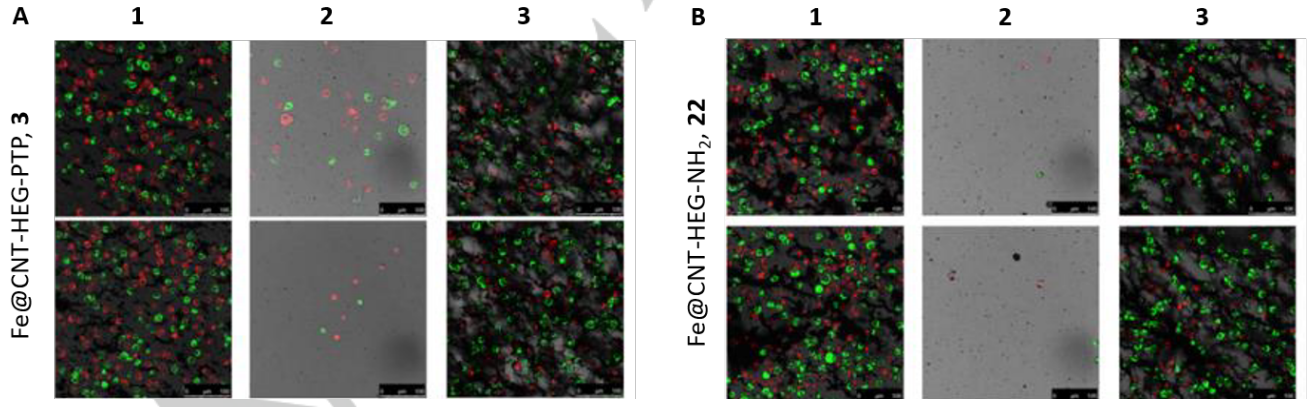

Figure 8. Confocal microscopy images of (1) an initial mixture of Fe@CNTs-HEG-PTP **3** (panel A) or Fe@CNTs-HEG-NH_2 **22** (panel B), CHO A_3AR (red) and CHO WT (green) cells and of the supernatant (2) and the magnetic precipitate (3) after 8 minutes of magnetic filtration.

Conclusion

The adenosine A_3 receptor holds an important role in cancer development and is over-expressed in a number of tumor tissues. In addition, the membrane localization of A_3ARs and their

existence in di- and oligomeric forms make them good candidates for a multivalent targeting cancer treatment. In this respect, this work focused on the conception of a novel multivalent Fe@CNTs tool conjugated to a small organic A_3AR ligand **1**, possessing a pyrazolo[4,3-*e*]-1,2,4-triazolo[1,5-*c*]-pyrimidine (PTP) core, for the selective targeting of human A_3AR-overexpressing cells. Our strategy involved the formation of a peptidic bond between Fe filled-CNTs and carboxylic acid **1** through two amino-terminated PEG spacers (TEG and HEG), giving Fe filled-CNTs-TEG-PTP (**2**) and Fe filled-CNTs-HEG-PTP (**3**). These conjugates showed good A_3AR binding affinity in binding studies (displacement > 80% at 10 µM) unlike control Fe filled-CNTs-PEG-NH_2 **21** and **22**, thus demonstrating that our conjugation strategy maintains the affinity of the ligand against its target. The ability of Fe filled-CNTs-HEG-PTP (**3**) to selectively target and shepherd A_3AR+ vs. A_3AR- cells was also evaluated *in vitro*. Interestingly, the opposite selectivity was observed. This effect was further investigated and ascribed to the formation of electrostatic interactions between unreacted cationic free amino groups on Fe filled-CNTs-HEG-PTP (**3**) and anionic residues on cell membranes. These findings further suggest that the surface chemistry is a key component of a nanomaterial for its ability to bind a receptor embedded in a cell membrane and thus the careful choice of the nanostructure exosurface functionalization has to be made.[54–57] Even if further development is needed to obtain a nano-tool able to shepherd A_3AR overexpressing cancer cells, this work opens the door to the investigation of new possible applications of Fe filled-CNTs in cancer treatment.

Experimental Section

General methods

Thin layer chromatography (TLC) was conducted on pre-coated aluminum sheets with 0.20 mm *Macherey-Nagel Alugram SIL G/UV254* with fluorescent indicator UV254. Column chromatography was carried out using *Merck Gerduran* silica gel 60 (particle size 40-63 µm). Melting points (M.p.) were measured on a *Büchi Melting Point B-545* in open capillary tubes and have not been corrected. Nuclear magnetic resonance (NMR) ^1H, ^{13}C spectra were obtained on a 500 MHz *(Jeol JNM ECZR-500)* or 400 MHz NMR *(Jeol JNM EX-400).* Chemical shifts were reported in ppm using the solvent residual signal as an internal reference. Coupling constants (J) were given in Hz. Resonance multiplicity was described as *s* (singlet), *d* (doublet), *t* (triplet), *dd* (doublet of doublets), *q* (quartet), *m* (multiplet) and *br* (broad signal). Carbon spectra were acquired with a complete decoupling for the proton. The *Delta 5* software (Jeol) was used for data processing. Infrared spectra (IR) were recorded on a *Perkin-Elmer Spectrum II FT-IR System* with *Specac* Silver Gate Evolution single-reflection ATR mounted with a diamond crystal. Mass spectrometry (MS) was performed either by the *Centre de spectrométrie de masse* at the *Université de Mons in Belgium* were they performed high-resolution ESI-MS (HRMS) and MALDI-MS, or by the *Fédération de Recherche ICOA/CBM (FR2708) platform of Orléans in France*, where they performed high-resolution ESI-MS (HRMS). ESI-MS measurements at the *Université de Mons* were performed on a *Waters QToF2 mass spectrometer* operating in positive mode. High-resolution ESI mass spectra (HRMS) at *Orléans* were performed on a *BrukermaXis Q-TOF* in the positive ion mode. Data were processed using *BrukerDataAnalysis 4.1* software. Thermogravimetric analyses (TGA) were performed using a *TGA Q500* (TA Instruments), treating the samples placed in Pt pans with the following procedure: isotherm at 100°C for 20 min (to remove residual solvent, if any), ramp from 100 to 800°C at 10°C·min^{-1}, under nitrogen or air (flow rate on the sample of 90 mL·min^{-1}). X-Ray photoelectron spectroscopy (XPS) analyses were performed on a *Thermo Scientific K-Alpha XPS system* (Thermo Fisher Scientific). For each analysis, about 0.5 mg of material were deposited on a copper thin film, which was then fixed on an XPS sample holder using a double side adhesive conductive carbon tap (SPI supplies). Spectra were collected using a monochromatized Al-K α radiation (1486.6 eV). The surface normal emitted photoelectron was analyzed in a double-focusing hemispherical analyzer and recorded on a multi-channel detector. All the spectra were acquired in the constant analyzer energy mode. The *Thermo Scientific Avantage* software (Thermo Fisher Scientific) was used for digital acquisition and data processing. Optical Microscopy images of cells were acquired with a *Leitz Labovert FS* optical microscope equipped with a *Leica DFC290* camera. Confocal Fluorescence Microscopy images of cells were acquired with a *Leica SP5* microscope. Elemental analysis (EA) (C,H,N) was performed on a *Thermo Finnigan-Flash EA 1112*.

Synthetic procedures

The Fe@CNTs used in this work are obtained by *in situ* procedure employing chemical vapour deposition methodology followed by washings with hydrochloric acid as reported in our previous work.[44] Compound **1** was obtained following previously reported procedures.[45,58]

Synthesis of 2-(2-(2-hydroxyethoxy)ethoxy)ethyl 4-methylbenzenesulfonate 8. To a solution of tri-ethyleneglycol (29.82 g, 0.199 mol) in THF (12.5 mL) was added a solution of sodium hydroxide (1.587 g, 0.0396 mol) in water (9.5 mL). The resulting mixture was stirred at room temperature for 10 min and then cooled at 0 °C. A solution of tosyl chloride (4.738 g, 0.0248 mol) in THF (31 mL) was added dropwise over 1 h, the resulting mixture stirred 2 hours at 0 °C, let warmed to room temperature and stirred for additional 4 hours. The reaction mixture was diluted with water (100 mL) and dichloromethane (50 mL) and the aqueous phase extracted with dichloromethane (5 × 50 mL), the combined organic layers were dried over magnesium sulfate, filtered and concentrated under reduced pressure to afford desired compound **8** as a yellow oil (7.450 g, 0.0245 mol, 99%). ^1H-NMR ($CDCl_3$): δ 7.79 (*d*, 2H, *J*=8.3 Hz), 7.33 (*d*, 2H, *J*=8.3 Hz), 4.17-4.15 (*m*, 2H), 3.72-3.57 (*m*, 10H), 2.44 (*s*, 3H). 1H peak missing. ^{13}C-NMR ($CDCl_3$): δ 144.98, 133.00, 129.94, 128.06, 72.69, 72.56, 70.87, 70.47, 70.39, 69.27, 68.79, 61.78, 21.75. Characterization in agreement with previously reported data.[59]

Synthesis of 17-hydroxy-3,6,9,12,15-pentaoxaheptadecyl 4-methylbenzenesulfonate 9. To a cooled (0 °C) solution of hexa-ethyleneglycol (10 g, 35.5 mmol) and triethylamine (2.8 mL, 20 mmol) in THF (100 mL) was added tosyl chloride (6.76 g, 35.4 mmol, 0.98 eq.) in small portions (about 100 mg). This mixture was allowed to reach room temperature and stirred overnight. The reaction mixture was diluted with chloroform (60 mL) and extracted with 1M HCl (3 × 60 mL), brine (1 × 60 mL), dried over magnesium sulfate and concentrated under reduced pressure. The crude was purified by silica gel chromatography (dichloromethane 100% to dichloromethane/methanol 95:5) to afford the desired compound **9** as a yellow oil (5.21 g, 12 mmol, 34%). ^1H-NMR ($CDCl_3$): δ 7.80 (*d*, 2H, *J*=8.1 Hz), 7.34 (*d*, 2H, *J*=8.1 Hz), 4.16-4.14 (*m*, 2H), 3.80-3.58 (*m*, 22H), 2.44 (*s*, 3H). 1H peak missing. ^{13}C-NMR ($CDCl_3$): δ 144.93, 133.06, 129.95, 128.12, 72.73, 70.81, 70.65, 70.62, 70.35, 69.42, 68.80, 67.80, 21.79. Peaks missing due to overlaps in the PEG region. Characterization in agreement with previously reported data.[60]

Synthesis of 2-(2-(2-azidoethoxy)ethoxy)ethan-1-ol 10. To a solution of tosylate **8** (5 g, 16.4 mmol) in anhydrous DMF (10 mL) was added sodium azide (10.68 g, 164.5 mmol) under a flux of argon. The resulting mixture was stirred at 60 °C for 5 hours, concentrated under reduced pressure and diluted with water (50 mL) and dichloromethane (50 mL). The aqueous phase was extracted with dichloromethane (5 X 50 mL) and the combined organic layers dried over magnesium sulfate and concentrated under reduced pressure to afford desired compound **10** as a yellow oil (2.325 g, 13.2 mmol, 81%). ^1H-NMR ($CDCl_3$): δ 3.72-3.66 (*m*, 8H), 3.61-3.59 (*m*, 2H), 3.39-3.37 (*m*, 2H), 2.38 (*br* s, 1H). ^{13}C-NMR ($CDCl_3$): δ 72.59, 70.76, 70.50,

70.16, 61.87, 50.75. Characterization in agreement with previously reported data.[61]

Synthesis of 17-azido-3,6,9,12,15-pentaoxaheptadecan-1-ol 11. To a solution of tosylate **9** (2 g, 4.58 mmol) in anhydrous DMF (4 mL) was added sodium azide (2 g, 30.8 mmol) under a flux of argon. The reaction mixture was stirred 20 hours at 60 °C, concentrated under reduced pressure and the crude suspended in dichloromethane and filtered through cotton. The precipitate was washed with several portions of dichloromethane and the filtrate concentrated under reduced pressure to afford desired compound **11** as a colorless oil (1.4074 g, 4.58 mmol, quantitative). ^{1}H-NMR ($CDCl_3$): δ 3.64-3.62 (*m*, 2H), 3.60-3.56 (*m*, 18H), 3.53-3.51 (*m*, 2H), 3.32-3.30 (*m*, 2H), 2.96 (*s*, 1H). ^{13}C-NMR ($CDCl_3$): δ 72.45, 70.53, 70.48, 70.44, 70.20, 69.91, 61.52, 50.54. Peaks missing due to overlaps in the PEG region. Characterization in agreement with previously reported data.[62]

Synthesis of 2-(2-(2-azidoethoxy)ethoxy)ethyl 4-methylbenzenesulfonate 12. To a solution of azide **10** (1.13 g, 6.45 mmol) and tosyl chloride (1.23 g, 6.45 mmol) in dichloromethane (11 mL) was added powdered potassium hydroxide (1.44 g, 25.8 mmol) in small portions. The reaction mixture was stirred at room temperature for 8 hours and poured in water (25 mL). The aqueous layer was extracted with dichloromethane (2 × 25 mL), the combined organic layers were dried over magnesium sulfate and concentrated under reduced pressure to afford desired compound **12** as a colorless oil (1.908 g, 5.79 mmol, 90%)**.** ^{1}H-NMR ($CDCl_3$): δ 7.79 (*d*, 2H, *J*=8.3 Hz), 7.34 (*d*, 2H, *J*=8.3 Hz), 4.15 (*m*, 2H), 3.70-3.57 (*m*, 8H), 3.37-3.34 (*m*, 2H), 2.43 (*s*, 3H). ^{13}C-NMR ($CDCl_3$): δ 144.94, 133.07, 129.93, 128.06, 70.89, 70.70, 70.18, 69.36, 68.87, 50.74, 21.73. Characterization in agreement with previously reported data.[63]

Synthesis of 17-azido-3,6,9,12,15-pentaoxaheptadecyl 4-methylbenzenesulfonate 13. To a solution of azido **11** (5.10 g, 16.6 mmol) and tosyl chloride (3.17 g, 16.6 mmol) in dichloromethane (11 mL) was added freshly powdered potassium hydroxide (3.64 g, 65.1 mmol) (crushed in a mortar) in small portions. The reaction mixture was stirred at room temperature for 8 hours. Then water (30 mL) was carefully added. The aqueous layer was extracted with dichloromethane (3 X 30 mL), the combined organic layers were dried over magnesium sulfate and concentrated under reduced pressure to afford desired compound **13** as a colorless oil (7.85 g, 17.0 mmol, quantitative). ^{1}H-NMR ($CDCl_3$): δ 7.79 (*d*, 2H, *J*=8.4 Hz), 7.34 (*d*, 2H, *J*=8.4 Hz), 4.17-4.15 (*m*, 2H), 3.69-3.58 (*m*, 20H), 3.38-3.36 (*m*, 2H), 2.45 (*s*, 3H). ^{13}C-NMR ($CDCl_3$): δ 144.92, 133.10, 129.94, 128.10, 70.85, 70.78, 70.73, 70.67, 70.14, 69.37, 68.79, 50.79, 21.76. Peaks missing due to overlaps in the PEG region. Characterization in agreement with previously reported data.[62]

Synthesis of 1-(2-(2-(2-azidoethoxy)ethoxy)ethoxy)-4-nitrobenzene 14. In a flask under argon containing tosylate **12** (1.9 g, 5.76 mmol), *para*-nitrophenol (1.201 g, 8.64 mmol) and potassium carbonate (1.19 g, 8.64 mmol) was added anhydrous DMF (5mL) *via* syringe. The reaction mixture was stirred at 60°C for 24 h, concentrated under reduced pressure and diluted with water (50 mL) and ethyl acetate (30 mL). The organic layer was washed with saturated sodium carbonate (5 × 50 mL), until the aqueous layer was colorless. The combined organic layers were dried over magnesium sulfate, filtered and concentrated under reduced pressure to afford desired compound **14** as a yellow oil (1.599 g, 5.40 mmol, 94 %). ^{1}H-NMR ($CDCl_3$): δ 8.21 (*d*, 2H, *J*=9.2 Hz), 6.99 (*d*, 2H, *J*=9.3 Hz), 4.23-4.21 (*m*, 2H), 3.91-3.89 (*m*, 2H), 3.76-3.74 (*m*, 2H), 3.70-3.64 (*m*, 4H), 3.39-3.37 (*m*, 2H). ^{13}C-NMR ($CDCl_3$): δ 163.98, 141.75, 126.02, 114.72, 71.09, 70.89, 70.29, 69.62, 68.32, 50.81. IR (cm^{-1}): *v* 500.6, 532.68, 556.5, 627.44, 634.87, 657.71, 691.16, 752.89, 847.63, 926.1, 1054.1, 1110.48, 1174.76, 1261.22, 1299.41, 1339.7, 1452.22, 1497.84, 1511.02, 1593.12, 1607.77, 1767.92, 2100.52, 2449.8, 2517.74, 2871.04, 3084.26, 3114.35, 3185.05. MS (HR-LCMS, ESI+): found 297.1194 $[M+H]^+$, $C_{12}H_{17}N_4O_5$ requires 297.1193.

Synthesis of 1-azido-17-(4-nitrophenoxy)-3,6,9,12,15-pentaoxaheptadecane 15. In a flask under argon containing tosylate **13** (105 mg, 0.227 mmol), *para*-nitrophenol (45.26 mg, 0.325 mmol) and potassium carbonate (44.85 mg, 0.325 mmol) was added anhydrous DMF (5mL) *via* syringe. The reaction mixture was stirred at 60 °C for 72 hours, concentrated under reduced pressure and diluted with dichloromethane (30 mL). The organic layer was washed with a 9:1 (v:v) mixture of a saturated solution of potassium carbonate and a solution of NaOH (4.8 M) (4 × 30 mL) until the aqueous layer was colorless. The combined organic layers were dried over magnesium sulfate, filtered concentrated under reduced pressure to afford desired compound as a colorless oil **15** (90 mg, 0.211 mmol, 92%). ^{1}H-NMR ($CDCl_3$): δ 8.13 (*d*, 2H, *J*=9.2 Hz), 6.93 (*d*, 2H, *J*=9.2 Hz), 4.17 (*m*, 2H), 3.84 (*m*, 2H), 3.69-3.60 (*m*, 18H), 3.33 (*m*, 2H). ^{13}C-NMR ($CDCl_3$): δ 163.86, 141.48, 125.80, 114.56, 70.84, 70.61, 70.55, 70.51, 69.97, 69.31, 68.19, 50.61. Peaks missing due to overlaps in the PEG region. IR (cm^{-1}): *v* 501.62, 657.38, 691.36, 752.98, 773.01, 847.67, 942.68, 1053.13, 1107.9, 1174.81, 1260.5, 1299.32, 1339.56, 1452.17, 1497.89, 1511.26, 1592.87, 1607.43, 2100.53, 2868.34. MS (HR-LCMS, ESI+): found 429.1978 $[M+H]^+$, $C_{18}H_{29}N_4O_8$ requires 429.1979.

Synthesis of 4-(2-(2-(2-aminoethoxy)ethoxy)ethoxy)aniline 16. To a solution of nitrobenzene **14** (1.383 g, 4.67 mmol) in methanol (78 mL) was added PtO_2 (21 mg, 0.092 mmol). The reaction mixture was stirred 24 h at room temperature under an atmosphere of hydrogen and then filtered through a pad of celite. The filtrate was concentrated under reduced pressure to afford desired compound **16** as a colorless oil (1.026 g, 4.27 mmol, 91%). ^{1}H-NMR (CD_3OD): δ 6.76-6.73 (*m*, 2H), 6.72-6.68 (*m*, 2H), 4.04-4.02 (*m*, 2H), 3.80-3.78 (*m*, 2H), 3.64-3.61 (*m*, 4H), 3.52-3.50 (*m*, 2H), 2.81 (*m*, 2H). 2H peaks missing. ^{13}C-NMR (CD_3OD): δ 153.31, 142.05, 118.03, 116.71, 73.47, 71.63, 71.23, 70.98, 69.21, 42.10. IR (cm^{-1}): *v* 519.4, 749.43, 826.53, 927.78, 1064.9, 1109.42, 1237.39, 1297.79, 1351.55, 1456. MS (HR-LCMS, ESI+): found 241.1546 $[M+H]^+$, $C_{12}H_{21}N_2O_3$ requires 241.1547.

Synthesis of 17-(4-aminophenoxy)-3,6,9,12,15-pentaoxaheptadecan-1-amine 17. To a solution of nitrobenzene **15** (1.541 g, 3.6 mmol) in methanol (78 mL) was added PtO_2 (16 mg, 0.072 mmol). The reaction mixture was stirred 24 hours at room temperature under an atmosphere of hydrogen and then filtered through a pad of celite. The filtrate was concentrated under reduced pressure to afford desired compound **17** as a colorless oil (1.245 g, 3.35 mmol, 93%). ^{1}H-NMR ($CDCl_3$): 6.72-6.70 (*m*, 2H), 6.60-6.58 (*m*, 2H), 4.01 (*m*, 2H), 3.76 (*m*, 2H), 3.68-3.56 (*m*, 18H), 3.45 (*m*, 2H), 2.82 (*br. s*, 2H). 1H peak missing. ^{13}C-NMR ($CDCl_3$): 151.82, 140.30, 116.28, 115.83, 70.72, 70.58, 70.55, 70.25, 70.24, 69.89, 41.72. Peaks missing due to overlaps in the PEG region. IR (cm^{-1}): *v* 519.18, 772.2, 827.74, 947.61, 1105.32, 1237.07, 1349.97, 1455.91, 1511.27, 1675.79, 2869.65, 3352.59. MS (HR-LCMS, ESI+): found 373.2330 $[M+H]^+$, $C_{18}H_{33}N_2O_6$ requires 373.2333.

Synthesis of *tert*-butyl (2-(2-(2-(4-aminophenoxy)ethoxy)ethoxy)ethyl)carbamate 4. To a solution of aniline **16** (950 mg, 3.95 mmol) in anhydrous THF (10 mL) was added di-*tert*-butyl dicarbonate (863 mg, 3.95 mmol). The resulting solution was stirred under argon for 15 hours at room temperature, concentrated under reduced pressure and purified by silica gel chromatography (SiO_2 150 mL, cyclohexane/ethyl acetate 5:5 to 0:10) to afford desired mono-protected derivative **4** (881 mg, 2.59 mmol, 66%) as a colorless oil (bis-Boc protected derivative has not been detected). ^{1}H-NMR (DMSO-D_6): δ 6.77 (*t*, 1H, *J*=6.0 Hz), 6.64 (*d*, 2H, *J*=8.1 Hz), 6.50 (*d*, 2H, *J*=8.1 Hz), 4.70 (*s*, 2H), 3.93-3.90 (*m*, 2H), 3.67-3.65 (*m*, 2H), 3.57-3.55 (*m*, 2H), 3.51-3.49 (*m*, 2H), 3.37 (*t*, 2H, *J*=6.0 Hz), 3.06 (*q*, 2H, *J*=6.0 Hz), 1.37 (*s*, 9H). ^{13}C-NMR (DMSO-D_6): δ 155.59, 149.25, 115.34, 115.02, 118.03, 77.59, 69.84, 69.52, 69.18, 67.54, 40.21, 28.24. Peaks missing due to overlaps in the PEG region (at 69.18 ppm). IR (cm^{-1}): *v* 473.07, 516.98, 641.28, 755.71, 781.48, 825.28, 942.46, 1065.3, 1107.17, 1124.99, 1170.83, 1238.96, 1274.03, 1331.27, 1365.8, 1391.52, 1455.85, 1511.04, 1629.86, 1702, 2871.74, 2928.71, 2975.02, 3355.18. MS (HR-LCMS, ESI+): found 341.2069 $[M+H]^+$, $C_{17}H_{29}N_2O_5$ requires 341.2071.

Synthesis of *tert*-butyl (17-(4-aminophenoxy)-3,6,9,12,15-pentaoxaheptadecyl)carbamate 5 and *tert*-butyl (4-((2,2-dimethyl-4-oxo-3,8,11,14,17,20-hexaoxa-5-azadocosan-22-yl)oxy)phenyl)carbamate 18. To a solution of aniline **17** (1.250 g, 3.4 mmol) in anhydrous THF (10 mL) was added di-*tert*butyl dicarbonate (747 mg, 3.4 mmol). The reaction mixture was stirred under argon for 16 h at room temperature. The solution was then concentrated under reduced pressure and the crude was purified by silica gel chromatography (SiO_2 200 mL, cyclohexane/ethyl acetate 5:5 to 0:10) to afford successively bis-Boc protected derivative **18** as a colorless oil (127 mg, 0.221 mmol, 6%) and mono-protected derivative **5** as a colorless oil (1.105 g, 2.34 mmol, 69%). **5**: ^{1}H-NMR ($CDCl_3$): δ 6.73-6.71 (*m*, 2H), 6.62-6.60 (*m*, 2H), 5.09 (*br. s*, 1H), 4.03-4.01 (*m*, 2H), 3.80-3.77 (*m*, 2H), 3.70-3.57 (*m*, 16H), 3.51-3.49 (*m*, 2H), 3.31-3.25 (*m*, 2H), 1.42 (*s*, 9H). 1H peak missing. ^{13}C-NMR ($CDCl_3$): δ 156.08, 152.02, 140.01, 116.50, 115.87, 79.16, 70.79, 70.65, 70.60, 70.55, 70.25, 65.94, 68.15, 40.39, 28.48. Peaks missing due to overlaps in the PEG region. IR (cm^{-1}): *v* 516.85, 757.04, 775.92, 824.36, 947.62, 1098.6, 1169.28, 1236.93, 1272.65, 1328.42, 1350.31, 1365.04, 1391.08, 1455.33, 1509.91, 1630.07, 1704.37, 2868.94, 3354.6. MS (HR-LCMS, ESI+): found 473.2856 $[M+H]^+$, $C_{23}H_{41}N_2O_8$ requires 473.2857. **16:** ^{1}H-NMR ($CDCl_3$): δ 7.23 (*m*, 2H), 6.83 (*m*, 2H), 6.45 (*br. s.*, 1H), 5.05 (*br. s.*, 1H), 4.08 (*m*, 2H), 3.82 (*m*, 2H), 3.69-3.50 (*m*, 18H), 3.29 (*m*, 2H), 1.49 (*s*, 9H), 1.43 (*s*, 9H). ^{13}C-NMR ($CDCl_3$): δ 156.14, 154.89, 153.26, 131.78, 120.50, 115.14, 80.32, 79.26, 70.90, 70.72, 70.69, 70.61, 70.33, 69.87, 67.87, 40.45, 28.54, 28.48. Peaks missing due to overlaps in the PEG region. IR (cm^{-1}): *v* 522.76, 734.89, 774.4, 804.07, 830.08, 948.02, 1011.64, 1027.11, 1049.96, 1103.5, 1158.47, 1228.45, 1365.49, 1391.43, 1412.49, 1454.67, 1512.62, 1712.79, 2870.2, 2974.04. MS (HR-LCMS, ESI+): found 573.3382 $[M+H]^+$, $C_{28}H_{49}N_2O_{10}$ requires 573.3382.

Synthesis of Fe-filled-CNTs-TEG-Boc 19. To a dispersion of Fe filled-CNTs (200 mg) in NMP (90 mL), obtained by 20 min of sonication, was added a solution of aniline **4** (144 mg, 0.423 mmol) in NMP (10 mL). After 15 min of sonication isoamyl nitrite (192 µL, 1.438 mmol) was added and the reaction stirred at 90 °C for 20 hours. The reaction mixture was filtered on fluoropore filter, the precipitate washed with ethyl acetate (50 mL) and dispersed in AcOEt by 1 min of sonication and filtered again on fluoropore. Three cycles of filtration-dispersion-filtration followed by washing with acetone and removal of the solvents under reduced pressure afforded desired compound as a black powder (195 mg). The complete characterization of this material is presented under *Results and Discussion* section.

Synthesis of Fe-filled-CNTs-HEG-Boc 20. To a dispersion of Fe filled-CNTs (600 mg) in NMP (290 mL), obtained by 20 min of sonication, was added a solution of aniline **5** (600 mg, 1.27 mmol) in NMP (10 mL). After 15 min of sonication isoamyl nitrite (578 µL, 4.32 mmol) was added and the reaction stirred at 90 °C for 20 hours The reaction mixture was filtered through fluoropore filters, the filtrate washed with ethyl acetate (50 mL), re-dispersed in ethyl acetate (100 mL) by 1 min of sonication and filtered again on fluoropore filters. Three cycles of filtration-redispersion-filtration followed by washing with acetone and removal of the solvents under reduced pressure afforded desired compound as a black powder (511 mg). The complete characterization of this material is presented under *Results and Discussion* section.

Synthesis of Fe filled-CNTs-TEG-NH_2 21. To a dispersion of Fe-filled-CNTs-TEG-Boc **19** (150 mg) in methanol (263 mL), obtained by 10 min of sonication, was added under vigorous stirring a concentrated 12 N HCl solution (37.5 mL) and the reaction stirred at room temperature for 16 hours. The reaction mixture was poured into water (250 mL) and the precipitate formed filtered on an omnipore filter, re-dispersed in methanol (25 mL), poured in water (100 mL) and filtered again on omnipore. Three successive filtration-redispersion-filtration cycles followed by a last washing with small amounts of methanol afforded desired compound as a black powder (150 mg). The complete characterization of this material is presented under *Results and Discussion* section.

Synthesis of Fe-filled-CNTs-HEG-NH_2 22. To a dispersion of Fe-filled-CNTs-HEG-Boc **20** (300 mg) in methanol (525 mL), obtained by 10 min of sonication, was added a concentrated 12 N HCl solution (75 mL) under vigorous stirring and the reaction stirred at room temperature for 16 h. The reaction mixture was poured into water (200 mL), the precipitate formed filtered on an omnipore filter, re-dispersed in methanol (50 mL), poured in water (200 mL) and filtered again on omnipore. Three successive filtration-redispersion-filtration cycles followed by a last washing with small amounts of methanol afforded desired compound as a black powder (290 mg). The complete characterization of this material is presented under *Results and Discussion* section.

Synthesis of dioxopyrrolidin-1-yl 2-(4-(3-(2-(furan-2-yl)-8-methyl-8H-pyrazolo[4,3-e][1,2,4]triazolo[1,5-c]pyrimidin-5-yl)ureido)phenyl)acetate 23. In a flask under argon containing PTP-COOH **1** (25 mg, 0.0578 mmol), N-hydroxysuccinimide (27 mg, 0.231 mmol), EDC·HCl (44.3 mg, 0.231 mmol) and DMAP (28.2 mg, 0.231 mmol) was added *via* syringe anhydrous DMF. The reaction mixture was sonicated for 30 sec, stirred for 48 hours at room temperature, concentrated under reduced pressure and diluted with water (25 mL) and ethyl acetate (50 mL). The aqueous phase was extracted with ethyl acetate (2 × 50 mL), the combined organic layers dried over magnesium sulfate, filtered and concentrated under reduced pressure. The crude was purified by silica gel chromatography (SiO_2 100 mL, ethyl acetate /acetonitrile 10:0 to 6:4) to afford desired compound **23** as a white solid (14 mg, 0.026 mmol, 44 %). This compound tends to quickly hydrolyze. As a consequence, it was kept under argon at -22 °C, always synthesized on the strictly necessary amounts and engaged as soon as possible in the next reaction. M.p.: 177°C (decomposition). ^{1}H-NMR (DMSO-D_6): 10.68 (*s*, 1H), 9.73 (*s*, 1H), 8.79 (*s*, 1H), 7.98 (*dd*, 1H, J_1=1.6, J_2=0.7), 7.57 (*d*, 2H, *J*=8.2 Hz), 7.37 (*d*, 2H, *J*=8.2 Hz), 7.30 (*dd*, 1H, J_1=3.4, J_2=0.7), 6.76 (*dd*, 1H, J_1=3.4, J_2=1.6), 4.14 (*s*, 3H), 4.09 (*s*, 2H), 2.82 (*s*, 4H). IR (cm^{-1}): *v* 472.53, 595.42, 646.37, 762.03, 813.29, 905.03, 974.76, 1014.53, 1068.35, 1120.7, 1186.49, 1207.38, 1237.48, 1317.96, 1422.21, 1511.97, 1612.15, 1673.64, 1736.93, 1782.93, 1812.67, 2853.87, 2924.14, 3126.64. MS (HR-LCMS, ESI+): found 530.1533 $[M+H]^+$, $C_{24}H_{20}N_9O_6$ requires 530.1531. Found 447.1524 $[M\text{-}OSu+OMe+H]^+$, $C_{21}H_{19}N_8O_4$ requires 447.1529.

Synthesis of Fe-filled-CNTs-TEG-PTP 2. To a dispersion of Fe filled CNTs-TEG-NH_2 (**21**, 30 mg) in anhydrous DMF (4mL), obtained by 10 min of sonication, were added succinimidic activated ester **23** (10 mg, 0.019 mmol) and triethylamine (10 µL, 0.072 mmol). The reaction mixture was sonicated 5 min more and stirred at room temperature for 14 hours, filtered on omnipore and rinsed with DMF (10 mL). The precipitate re-dispersed by 1 min of sonication in methanol and filtered again. Three cycles of redispersion-filtration afforded desired material as a black powder (29 mg). The complete characterization of this material is presented under *Results and Discussion* section.

Synthesis of Fe-filled-CNTs-HEG-PTP 3. To a dispersion of Fe filled CNTs-HEG-NH_2 (**22,** 30 mg) in anhydrous DMF (6mL), obtained by 10 min of sonication, were added activated succinimidic ester **23** (10 mg, 0.019 mmol) and triethylamine (10 µL, 0.072 mmol). The reaction mixture was sonicated 5 min more, stirred at room temperature for 14 hours, filtered through omnipore and rinsed with DMF (10 mL) and the precipitate was re-dispersed by 1 min of sonication in methanol and filtered again. Three cycles of redispersion-filtration afforded desired material as a black powder (31 mg). The complete characterization of this material is presented under *Results and Discussion* section.

Radioligand competition experiments. Radioligand binding experiment with [^{3}H]HEMADO were performed according to previously reported procedures.[49,50] Parts of the detailed protocol are reproduced here:

Crude membranes for radioligand binding experiments were prepared by thawing frozen A_3AR-overexpressing CHO cells followed by scraping them off the petri dishes in ice-cold hypotonic buffer (5mM Tris/HCl, 2 mM EDTA, pH 7.4). The cell suspension was homogenized on ice (Ultra-Turrax, 2 X

15 s at full speed) and the homogenate was spun for 10 min (4 °C) at 1,000 g. The supernatant was then centrifuged for 30 min at 100,000 g. The membrane pellet was resuspended in 50 mM Tris/HCl, 10 mM $MgCl_2$, 1 mM EDTA, pH 8.25, frozen in liquid nitrogen at a protein concentration of 1–3 mg·ml^{-1} and stored at -80 °C. For incubation and separation of bound from free radioligand a 96-well microplate filtration system with built in filter bottoms (Millipore Multiscreen MAFC) was used.[49] Competitions binding studies were done at a concentration of 1 nM of [^{3}H]HEMADO, incubated in duplicates with different concentrations (0.3, 1, 3 and 10 µM) of Fe filled-CNTs-PEG-PTP (**2,3**), Fe filled-CNTs-PEG-NH_2 (**21,22**) or TEG-PTP **6** and HEG-PTP **7** for 3 hours at 25 °C (for CNTs, the concentrations are based on calculated PTP content or on the same weight amount as for the derivatized material for control Fe filled-CNTs-PEG-NH_2 (**21,22**)). The samples were then filtered through the built-in filter at the bottom of the wells and washed three times with 200 µL of ice-cold binding buffer. After addition of 20 µL of scintillator to the dried filter plates samples were counted in a beta counter. *Ki* values were calculated from competition curves by nonlinear curve fitting with the program Prism 6 (GraphPad Software).

Magnetic cell sorting. 400 µL of a 430,000 cells·mL^{-1} suspension in complete CO_2 independent medium was added to 113 µL of Fe filled-CNTs-HEG-PTP (**3**) (dispersed at a constant concentration of 1200 µg·mL-1 by 60 sec of sonication in complete CO_2 independent medium). The resulting mixture was diluted to 1000 µL with complete CO_2 independent medium and mixed for 10 min in a plastic vial, giving a final concentration of 215,000 cells·mL^{-1} and 172 µg CNTs·mL^{-1}. Then, a Ne-B permanent magnet (4X4X2 cm, *Supermagnete*) was placed against the vial and 100 µL supernatant aliquots were removed after 1, 2, 4 and 8 min of magnetic sorting. These aliquots were centrifuged in eppendorfs (3 min, 5000 rpm). The first 75 µL of the supernatant were discarded and the remaining pellet (25 µL) was re-dispersed. Cells in this pellet were counted (and imaged) in a Neubauer chamber.

Magnetic sorting of a mixture of CHO wild-type and CHO A_3 cells. 5 µL of fluorescent dye (DII for CHO A_3, red, DIO for CHO WT, green) were added to 1 mL of 1,500,000 cells·mL^{-1} CHO WT or CHO A_3 cells suspension in CO_2 independent medium. After 25 min of agitation on a planetary rotator at 37 °C protected from light, the two samples were subjected to three cycles of centrifugation at 1500 rpm for 5 min. After medium removal and resuspension in 1 mL of CO_2 independent medium, the cells were counted, re-adjusted to 1,500,000 cells·mL^{-1}, and used for the magnetic filtration test. In a 1.5 plastic vial, 250 µL of the CHO WT cells suspension, 250 µL of the CHO A_3 cells suspension and 250 µL of a 1200 µg·mL^{-1} dispersion of Fe filled-CNTs-HEG-PTP (**3**) were mixed with 250 µL of CO_2 independent medium, giving a total volume of 1 mL and final cell densities of 375,000 A431 cells·mL^{-1}, 375,000 EA cells·mL^{-1} and a CNTs concentration of 300 µg·mL^{-1}. 200 µL of this solution were withdrawn at *t0* for the confocal analysis. The cell suspension was then agitated for 10 min. Then, a Ne-B permanent magnet (4X4X2 cm, *Supermagnete*) was placed against the vial and 200 µL of supernatant were removed after 8 min of magnetic sorting for confocal analysis. After complete removal of the supernatant, the magnetic precipitate was re-dispersed in 400 µL of CO_2 independent medium and used for confocal analysis.

Computational Studies. CNT coordinates were modeled by using Nanotube builder tool of VMD package as a single wall, uncapped at the terminal, and empty nanotube.[64] A segment of a nanotube of 35 nm in length was generated by setting chiral indexes, n and m, to 60 and 60 respectively. The CNT was then functionalized with the spacers and the PTP derivative with MOE modeling suite.[65] A previously proposed homology model of the hA_3AR based on the crystallographic structure of $hA_{2A}AR$ in complex with the antagonist ZM241385 (PDB code: 3EML) was used for modeling studies.[66,67]

The PTP derivative coordinates inside the hA_3AR binding site were obtained by a molecular docking simulation with GOLD protocol according to previous studies on the binding mode of PTP based antagonist.[47,68] The CNT were manually placed in the proximity of the linkers and connected to reproduce the synthesis route. A series of minimizations was then performed on the linker and successively on the system with MOE minimization tool adopting amber10:ETH force field. Finally, the receptor-CNTs-PEG-PTP complex was embedded in a 1-palmitoyl-2oleyl-sn-glycerol-3-phospho-choline (POPC) lipid bilayer, based on the pre-orientation provided by the Orientations Proteins in Membrane (OPM) database.[69]

.

Acknowledgements

MMS lab is very grateful to Chemical Computing Group, OpenEye, and Acellera for the scientific and technical partnership. MMS lab gratefully acknowledges the support of NVIDIA Corporation with the donation of the Titan V GPU used for this research. The authors thank the Morph-Im UNamur technological platform.

Keywords: G protein-coupled receptor • A_3 adenosine receptor • carbon nanotubes • docking • theranostic • cancer • magnetic cell sorting

[1] J.-F. Chen, H. K. Eltzschig, B. B. Fredholm, *Nat. Rev. Drug Discov.* **2013**, *12*, 265–286.

[2] R. A. Cunha, *J. Neurochem.* **2016**, *139*, 1019–1055.

[3] W. Geldenhuys, A. Hanif, J. Yun, M. Nayeem, W. J. Geldenhuys, A. Hanif, J. Yun, M. A. Nayeem, *Molecules* **2017**, *22*, 917.

[4] M. H. Kazemi, S. Raoofi Mohseni, M. Hojjat-Farsangi, E. Anvari, G. Ghalamfarsa, H. Mohammadi, F. Jadidi-Niaragh, *J. Cell. Physiol.* **2018**, *233*, 2032–2057.

[5] K. A. Jacobson, S. Merighi, K. Varani, P. A. Borea, S. Baraldi, M. Aghazadeh Tabrizi, R. Romagnoli, P. G. Baraldi, A. Ciancetta, D. K. Tosh, Z. G. Gao, S. Gessi, *Med. Res. Rev.* **2018**, *38*, 1031–1072.

[6] B. B. Fredholm, a P. IJzerman, K. a Jacobson, K. N. Klotz, J. Linden, *Pharmacol. Rev.* **2001**, *53*, 527–552.

[7] D. Vijayan, A. Young, M. W. L. Teng, M. J. Smyth, *Nat. Rev. Cancer* **2017**, *17*, 709–724.

[8] B. B. Fredholm, *Cell Death Differ.* **2007**, *14*, 1315–1323.

[9] S. Muller-Haegele, L. Muller, T. L. Whiteside, *Expert Rev. Clin. Immunol.* **2014**, *10*, 897–914.

[10] G. Ohana, S. Bar-Yehuda, A. Arich, L. Madi, Z. Dreznick, L. Rath-Wolfson, D. Silberman, G. Slosman, P. Fishman, *Br. J. Cancer* **2003**, *89*, 1552–1558.

[11] Y. Kohno, Y. Sei, M. Koshiba, H. O. Kim, K. A. Jacobson, *Biochem. Biophys. Res. Commun.* **1996**, *219*, 904–910.

[12] S. Gessi, V. Sacchetto, E. Fogli, S. Merighi, K. Varani, P. G. Baraldi, M. A. Tabrizi, E. Leung, S. Maclennan, P. A. Borea, *Biochem. Pharmacol.* **2010**, *79*, 1483–95.

[13] M. Mujoomdar, D. Hoskin, J. Blay, *Biochem. Pharmacol.* **2003**, *66*, 1737–1747.

[14] P. Fishman, S. Bar-Yehuda, E. Ardon, L. Rath-Wolfson, F. Barrer, A. Ochaion, L. Madi, *Anticancer Res.* **2003**, *23*, 2077–2083.

[15] L. Madi, S. Bar-Yehuda, F. Barer, E. Ardon, A. Ochaion, P. Fishman, *J. Biol. Chem.* **2003**, *278*, 42121–42130.

[16] S. Gessi, E. Cattabriga, A. Avitabile, R. Gafa, G. Lanza, L. Cavazzini, N. Bianchi, R. Gambari, C. Feo, A. Liboni, S. Gullini, E. Leung, S. Mac-Lennan, P. A. Borea, *Clin Cancer Res* **2004**, *10*,

5895–5901.

[17] L. Madi, A. Ochaion, L. Rath-Wolfson, S. Bar-Yehuda, A. Erlanger, G. Ohana, A. Harish, O. Merimski, F. Barer, P. Fishman, *Clin. Cancer Res.* **2004**, *10*, 4472–4479.

[18] L. T. May, L. J. Bridge, L. a Stoddart, S. J. Briddon, S. J. Hill, *FASEB J.* **2011**, *25*, 3465–76.

[19] S. J. Hill, L. T. May, B. Kellam, J. Woolard, *Br. J. Pharmacol.* **2014**, *171*, 1102–1113.

[20] N. J. Smith, G. Milligan, **2010**, *62*, 701–725.

[21] D. K. Tosh, L. S. Yoo, M. Chinn, K. Hong, S. M. Kilbey, M. O. Barrett, I. P. Fricks, T. K. Harden, Z. G. Gao, K. A. Jacobson, *Bioconjug. Chem.* **2010**, *21*, 372–384.

[22] Y. Kim, B. Hechler, A. M. Klutz, C. Gachet, K. a Jacobson, *Bioconjug. Chem.* **2008**, *19*, 406–411.

[23] A. a. Ivanov, K. a. Jacobson, *Bioorg. Med. Chem. Lett.* **2008**, *18*, 4312–4315.

[24] A. Kecskés, D. K. Tosh, Q. Wei, Z.-G. Gao, K. a Jacobson, *Bioconjug. Chem.* **2011**, *22*, 1115–27.

[25] T. C. Wan, D. K. Tosh, L. Du, E. T. Gizewski, K. A. Jacobson, J. A. Auchampach, *BMC Pharmacol.* **2011**, *11*, 11.

[26] B. Chanyshev, A. Shainberg, A. Isak, A. Litinsky, Y. Chepurko, D. K. Tosh, K. Phan, Z.-G. Gao, E. Hochhauser, K. A. Jacobson, *Pharmacol. Res.* **2012**, *65*, 338–346.

[27] P. S. Jayasekara, K. Phan, D. K. Tosh, T. S. Kumar, S. M. Moss, G. Zhang, J. J. Barchi, Z.-G. Gao, K. A. Jacobson, K. A. Jacobson, *Purinergic Signal.* **2013**, *9*, 183–198.

[28] X. Ma, Y. Xiong, L. Lee, X. Ma, Y. Xiong, L. T. O. Lee, *Int. J. Mol. Sci.* **2018**, *19*, 2006.

[29] S. Federico, G. Spalluto, *Future Med. Chem.* **2019**, *11*, 1673–1677.

[30] M. Mohajeri, B. Behnam, A. Sahebkar, *J. Cell. Physiol.* **2018**, *234*, 298–319.

[31] B. Pelaz, C. Alexiou, R. A. Alvarez-Puebla, F. Alves, A. M. Andrews, S. Ashraf, L. P. Balogh, L. Ballerini, A. Bestetti, C. Brendel, S. Bosi, M. Carril, W. C. W. Chan, C. Chen, X. Chen, X. Chen, Z. Cheng, D. Cui, J. Du, C. Dullin, A. Escudero, N. Feliu, M. Gao, M. George, Y. Gogotsi, A. Grünweller, Z. Gu, N. J. Halas, N. Hampp, R. K. Hartmann, M. C. Hersam, P. Hunziker, J. Jian, X. Jiang, P. Jungebluth, P. Kadhiresan, K. Kataoka, A. Khademhosseini, J. Kopeček, N. A. Kotov, H. F. Krug, D. S. Lee, C.-M. Lehr, K. W. Leong, X.-J. Liang, M. Ling Lim, L. M. Liz-Marzán, X. Ma, P. Macchiarini, H. Meng, H. Möhwald, P. Mulvaney, A. E. Nel, S. Nie, P. Nordlander, T. Okano, J. Oliveira, T. H. Park, R. M. Penner, M. Prato, V. Puntes, V. M. Rotello, A. Samarakoon, R. E. Schaak, Y. Shen, S. Sjöqvist, A. G. Skirtach, M. G. Soliman, M. M. Stevens, H.-W. Sung, B. Z. Tang, R. Tietze, B. N. Udugama, J. S. VanEpps, T. Weil, P. S. Weiss, I. Willner, Y. Wu, L. Yang, Z. Yue, Q. Zhang, Q. Zhang, X.-E. Zhang, Y. Zhao, X. Zhou, W. J. Parak, *ACS Nano* **2017**, *11*, 2313–2381.

[32] K. Kostarelos, A. Bianco, M. Prato, *Nat. Nanotechnol.* **2009**, *4*, 627–633.

[33] S. Marchesan, K. Kostarelos, A. Bianco, M. Prato, *Mater. Today* **2015**, *18*, 12–19.

[34] M. Martincic, G. Tobias, *Expert Opin. Drug Deliv.* **2015**, *12*, 563–581.

[35] N. Do Quyen Chau, C. Ménard-Moyon, K. Kostarelos, A. Bianco, *Biochem. Biophys. Res. Commun.* **2015**, *468*, 454–462.

[36] A. Battigelli, C. Ménard-Moyon, T. Da Ros, M. Prato, A. Bianco, *Adv. Drug Deliv. Rev.* **2013**, *65*, 1899–1920.

[37] N. Martín, T. Da Ros, J.-F. Nierengarten, *J. Mater. Chem. B* **2017**, *5*, 6425–6427.

[38] H. Liu, L. Zhang, M. Yan, J. Yu, *J. Mater. Chem. B* **2017**, *5*, 6437–6450.

[39] L. Rodríguez-Pérez, J. Ramos-Soriano, A. Pérez-Sánchez, B. M. Illescas, A. Muñoz, J. Luczkowiak, F. Lasala, J. Rojo, R. Delgado, N. Martín, *J. Am. Chem. Soc.* **2018**, *140*, 9891–9898.

[40] A. Stopin, F. Pineux, R. Marega, D. Bonifazi, *Chem. - A Eur. J.* **2015**, *21*, 9288–9301.

[41] R. Marega, D. Bonifazi, *New J. Chem.* **2014**, *38*, 22–27.

[42] M. Melchionna, A. Beltram, A. Stopin, T. Montini, R. W. Lodge, A. N. Khlobystov, D. Bonifazi, M. Prato, P. Fornasiero, *Appl. Catal. B Environ.* **2018**, *227*, 356–365.

[43] R. Marega, F. De Leo, F. Pineux, J. Sgrignani, A. Magistrato, A. D. Naik, Y. Garcia, L. Flamant, C. Michiels, D. Bonifazi, *Adv. Funct. Mater.* **2013**, *23*, 3173–3184.

[44] F. Pineux, R. Marega, A. Stopin, A. La Torre, Y. Garcia, E. Devlin, C. Michiels, A. N. Khlobystov, D. Bonifazi, *Nanoscale* **2015**, *7*, 20474–20488.

[45] K. A. Jacobson, K. S. Thatikonda, E. E. Kozma, G. Spalluto, S. Moro, S. Federico, *Fluorescent Antagonists of the A3 Adenosine Receptor*, **2016**, US9227979B2.

[46] F. De Leo, J. Sgrignani, D. Bonifazi, A. Magistrato, *Chem. - A Eur. J.* **2013**, *19*, 12281–12293.

[47] E. Kozma, T. S. Kumar, S. Federico, K. Phan, R. Balasubramanian, Z.-G. Gao, S. Paoletta, S. Moro, G. Spalluto, K. A. Jacobson, *Biochem. Pharmacol.* **2012**, *83*, 1552–1561.

[48] J. L. Bahr, J. M. Tour, *Chem. Mater.* **2001**, *13*, 3823–3824.

[49] K.-N. Klotz, J. Hessling, J. Hegler, C. Owman, B. Kull, B. B. Fredholm, M. J. Lohse, *Naunyn. Schmiedebergs. Arch. Pharmacol.* **1998**, *357*, 1–9.

[50] K. N. Klotz, N. Falgner, S. Kachler, C. Lambertucci, S. Vittori, R. Volpini, G. Cristalli, *Eur. J. Pharmacol.* **2007**, *556*, 14–18.

[51] S. E. Kornguth, T. Kalinke, H. I. Robins, J. D. Cohen, P. Turski, *Cancer Res.* **1989**, *49*, 6390–5.

[52] N. S. Soukos, M. R. Hamblin, T. Hasan, *Photochem. Photobiol.* **1997**, *65*, 723–729.

[53] R. Frost, C. Grandfils, B. Cerda, B. Kasemo, S. Svedhem, *J. Biomater. Nanobiotechnol.* **2011**, *2*, 181–193.

[54] F. De Leo, A. Magistrato, D. Bonifazi, *Chem. Soc. Rev.* **2015**, *44*, 6916–6953.

[55] S. Marchesan, M. Prato, *Chem. Commun.* **2015**, *51*, 4347–4359.

[56] M. Calvaresi, F. Zerbetto, *Acc. Chem. Res.* **2013**, *46*, 2454–2463.

[57] G. Zuo, Q. Huang, G. Wei, R. Zhou, H. Fang, *ACS Nano* **2010**, *4*, 7508–7514.

[58] S. Moro, P. Braiuca, F. Deflorian, C. Ferrari, G. Pastorin, B. Cacciari, P. G. Baraldi, K. Varani, P. A. Borea, G. Spalluto, *J. Med. Chem.* **2005**, *48*, 152–162.

[59] M. Billamboz, F. Mangin, N. Drillaud, C. Chevrin-Villette, E. Banaszak-Léonard, C. Len, *J. Org. Chem.* **2014**, *79*, 493–500.

[60] A. Dif, F. Boulmedais, M. Pinot, V. Roullier, M. Baudy-Floc'h, F. M. Coquelle, S. Clarke, P. Neveu, F. Vignaux, R. Le Borgne, M. Dahan, Z. Gueroui, V. Marchi-Artzner, *J. Am. Chem. Soc.* **2009**, *131*, 14738–14746.

[61] T. Uppal, N. V. S. D. K. Bhupathiraju, M. G. H. Vicente, *Tetrahedron* **2013**, *69*, 4687–4693.

[62] D. J. Vugts, A. Vervoort, M. Stigter-van Walsum, G. W. M. Visser, M. S. Robillard, R. M. Versteegen, R. C. M. Vulders, J. (Koos) D. M. Herscheid, G. A. M. S. van Dongen, *Bioconjug. Chem.* **2011**, *22*, 2072–2081.

[63] E. Fernandez-Megia, J. Correa, I. Rodríguez-Meizoso, R. Riguera, *Macromolecules* **2006**, *39*, 2113–2120.

[64] W. Humphrey, A. Dalke, K. Schulten, *J Mol Graph* **1996**, *14*, 27, 33–38.

[65] Chemical Computing Group (CCG) Inc., **2016**.

[66] M. Floris, D. Sabbadin, R. Medda, A. Bulfone, S. Moro, *Eur J Med Chem* **2012**, *58*, 248–257.

[67] V.-P. V.-P. Jaakola, M. T. Griffith, M. A. Hanson, V. Cherezov, E. Y. T. Chien, J. R. Lane, A. P. IJzerman, R. C. Stevens, *Science (80-.).* **2008**, *322*, 1211–1217.

[68] G. Jones, P. Willett, R. C. Glen, A. R. Leach, R. Taylor, *J Mol Biol* **1997**, *267*, 727–748.

[69] M. A. Lomize, A. L. Lomize, I. D. Pogozheva, H. I. Mosberg, *Bioinformatics* **2006**, *22*, 623–625.

Entry for the Table of Contents

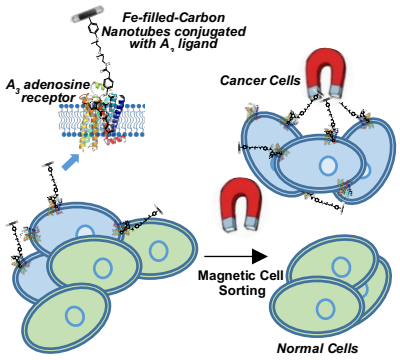

A_3 adenosine receptor ligands conjugated to Fe-filled carbon nanotubes were developed with the aim to target specific cancer cell lines for cancer magnetic cell sorting and thermal therapy. The nanostructure was able to efficiently bind to A_3 adenosine receptors, unfortunately, when interfaced with cells, the conjugates did not displayed selectivity for those overexpressing the receptor.

Institute and/or researcher Twitter usernames: @UniTrieste @UniPadova @UNamur @univienna @Uni_WUE